IEEE Access
Multidisciplinary | Rapid Review | Open Access Journal

Received November 21, 2019, accepted December 7, 2019, date of publication December 17, 2019,
date of current version December 26, 2019.

Digital Object Identifier 10.1109/ACCESS.2019.2960386

A Measuring Method for Nano Displacement Based on Fusing Data of Self-Sensing and Time-Digit-Conversion

ZHANGMING DU[1,2], CHAO ZHOU[1], TIANLU ZHANG[1,2], LU DENG[3], ZHIQIANG CAO[1], (Senior Member, IEEE), AND LONG CHENG[1,2], (Senior Member, IEEE)

[1]Institute of Automation, Chinese Academy of Sciences, Beijing 100190, China
[2]University of Chinese Academy of Sciences, Beijing 100049, China
[3]School of Statistics and Mathematics, Central University of Finance and Economics, Beijing 100081, China

Corresponding author: Chao Zhou (chao.zhou@ia.ac.cn)

This work was supported in part by the National Natural Science Foundation of China under Grant 61473295.

ABSTRACT Accurate and rapid measuring methods for displacement of nano-scale is necessary for manipulation. Self-sensing and time-digit-conversion(TDC) are two applicable measuring methods especially suitable for room-limited workspaces and vacuum-compliance required applications, thanks to their space-saving advantage and slight thermal impact on system. The self-sensing method gives measurements in high resolution at high sampling rate but its accuracy suffers from nonlinearity, while TDC has better linearity which causes less deviation to results but has a much lower sampling rate. A Kalman filter based fusion approach with dual estimation modes and self-adaptive parameters is designed to fuse the two measurements with different sampling rates at a higher frequency. Modifications to error covariance parameters are applied to traditional Kalman filter so that sensors' generalized errors rather than their Gaussian noises are taken into consideration, and corresponding derivation is given. A series of experiments are conducted to evaluate the performance of the fused measurement.

INDEX TERMS Nano-scale measurement, multi-rate fusion, self-sensing, TDC.

I. INTRODUCTION

Nanomanipulation plays an important role in nanotech which observes and controls matter in nano scale, enabling novel applications which depend on unique characteristics appearing in such small dimension. In a nanomanipulation system, accurate and rapid displacement sensing is a key technology for precise motion control.

Acquiring position information from vision feedbacks provided by high-resolution imaging devices such as scanning electron microscope (SEM) is a promising way used in automatical manipulation applications [1]–[4]. However, some applications also demand depth information in Z direction vertical to the visual field [3], which is hard to acquire from image. And for manipulators consisting of several actuators [5]–[7], it is necessary to build a closed loop for every degree-of-freedom(DOF), which demands displacement feedbacks of each actuator. But the highly magnified images are usually too distorted to provide accurate feedbacks, so other methods are necessary for each DOF's measurement as supplement.

Solutions based on different principles are proposed for displacement measurement. A widely-used strategy is to measure the distance between targets and a benchmark. Approaches in this form include laser interferometers, eddy-current sensors and capacitive sensors. Laser interferometers combined with mirror systems or fiber-optic [8]–[10], can provide extremely accurate measurement, in a resolution under 100 picometers [1]. However, it is a challenge to build a complex auxiliary optic system and fit it into the workspace of nano manipulator which is usually space-limited. Furthermore, if used inside an electronic microscope's vacuum chamber, the heat produced by laser will be hard to be dissipated thus will cause thermal drifts [11]. As a result, Laser-based methods are more suitable for sensor calibration rather than directly providing feedbacks in applications. Eddy-current sensors [12] operates on principle of electromagnetic induction, demanding the bulky probes staying close

The associate editor coordinating the review of this manuscript and approving it for publication was Hui Xie.

to targets one-on-one, limiting its use in many occasions. Capacitive sensors [12], [13] acquire displacement by measuring the capacitance changing along with the distance between the object and a nearby benchmark surface where the electrode plates should be accurately fixed, which is hard to be satisfied in many applications. Optical encoder-based sensors [14] have similar difficulty in assembly, and also generate heat that can cause thermal impact in vacuum workspace [1]. As the roles of nano actuators in most occasions are served by piezoelectric actuators(PEA) that deforms on principle of converse piezoelectric effect [15], measuring the strain when the PEA stretches and retracts is also a feasible way to acquire displacement. Corresponding approaches include strain gauge based methods [16], [17] and self-sensing methods [18]–[21]. With resistance changing along with deformation, strain gauges are low-cost, small-volume and easy to be mounted without strict requirement of assembly precision. The accuracy of this method is decided by the measurements for resistance of strain gauges. However, in traditional methods, the current flowing through strain gauges should be large enough to be sampled in high resolution, which also produces too much heat to cause thermal drift [11]. The newly reported PVDF method [22] utilizing piezoelectric polymer to sense the strain, overcoming the heat problem but has poor long stability. Another method, namely self-sensing, based on the unique property of piezoelectric materials, utilizes the inner relationship among strain and other physical variables to measure displacement. The strain can be sensed by outer circuits sampling on the driving circuit of actuator, making piezoelectric material both the actuator and the sensor in same time. Thus no additional probes or detectors are needed and little extra heat will be produced inside workspaces of nanomanipulator. As the sensor is actuator itself, the sensor-actuator pair is truly collocated [18], which means the mechanical errors introduced from assembly and external disturbance is eliminated.

This paper proposed a joint measurement combining a strain gauge based method named Time-Digit-Conversion (TDC) [11] and a self-sensing method. TDC indirectly measures the resistance of strain gauge by converting current measuring into time measuring. Compared to traditional strain gauge based methods, TDC produces much less heat thus is vacuum-compatible. Though TDC has better accuracy in general than the self-sensing, its sampling rate is too low for rapid motion applications. Compared to TDC, self-sensing has a much higher sampling rate and smaller noises, but suffers more from nonlinearity which affects its accuracy. Though observers with priori models can be used to improve accuracy [23], complex modeling is not necessary because of the participation of TDC. This paper designed a self-sensing method based on simultaneous measurement on both charge and voltage, with compensations for nonlinearity.

To combine the advantages and compensate the weakness of these two complementary measurements, a fusing method is needed to get a reliable estimation of displacement. Kalman filters are widely used for data fusion. However, as mentioned above, the two measurements are asynchronous with different sampling rates, while applications usually demand feedback as rapid as possible, which is a challenge for traditional Kalman filter. To solve the problem, variants of Kalman filter with special filter-designs [24]–[28] are proposed. Filters should be modified according to the traits of different data sources. However, few designs are aiming for fusing nano measurements like TDC and self-sensing, while measurements in nano scale can be very different. For example, Kalman filtering assumes that errors of raw data mainly caused by zero-mean Gaussian noises, that is not very true in nano scale measurement, which calls for more modification. Mixed methods combining Kalman filter with neural network [29] are also developed, utilizing the fitting ability of neural networks to fuse raw data into expected result, but the robustness of this kind of method highly depends on the completeness of training, and neural networks also require more computing resources.

In this paper, a dual-mode Kalman filter is proposed, of which the models are specially designed for each data source, and the generalized errors of original measurements rather than their noises are taken into consideration when calculating sensors' error covariance, which will be presented by a derivation. A self-adaptive modification is also used to secure the stability of the fusion. The fusion effectively combines the advantages of self-sensing and TDC, improving performance in displacement measurement.

II. MEASURING METHODS

A. SELF-SENSING METHOD

1) PRINCIPLE

As previously mentioned, self-sensing method adds no probes or detectors to actuator's workspace but only connects a sensing circuit to the driver of actuator, which can be deployed outside the workspace, emitting nearly no extra heat into it. The ability is achieved by taking advantage of inverse piezoelectric effect itself. The inner relationship among strain and other variables makes this method stable against external noises.

Self-sensing method can be educed from piezoelectric constitutive equations [30], [31], which present the relationships among strain S, electric displacement D, stress T, and electric field intensity E:

$$\begin{cases} S_m = \sum_i s_{im} T_i + \sum_j d_{jm} E_j \\ D_n = \sum_i d_{ni} T_i + \sum_j \epsilon_{nj} E_j \end{cases} \tag{1}$$

Here s_{im} is elastic compliance constant, ϵ_{nj} is dielectric constant, d_{jm} and d_{nj} are piezoelectric coefficient. The subscripts $m, n, i, j = 1, 2, 3$, indicate the normal directions of a cuboid piezoelectric stack's surfaces. They are directions where deformation happens, also the directions external forces and electric field act on. As all these electrical and mechanical factors are mainly applied in same directions in our case, most terms in (1) can be ignored [32], so the

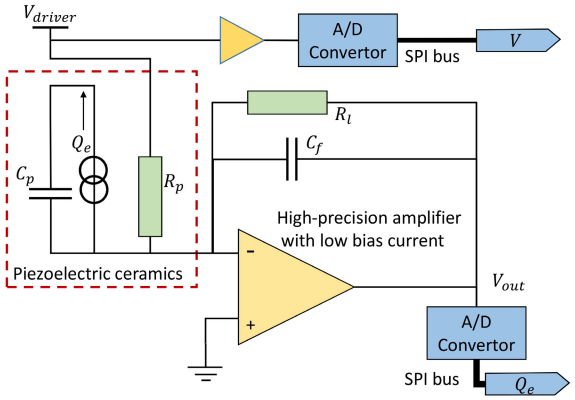

FIGURE 1. Schematic diagram of self-sensing method, parts inside the dashed box is the model of piezoelectric actuator (PEA).

equations are simplified as:

$$\begin{cases} S_1 = s_{11}T_1 + d_{11}E_1 \\ D_1 = d_{11}T_1 + \epsilon_{11}E_1 \end{cases} \tag{2}$$

Substitute T_1 in (2), we have:

$$S_1 = \frac{s_{11}}{d_{11}} \cdot D_1 + (d_{11} - \frac{s_{11}\epsilon_{11}}{d_{11}}) \cdot E_1 \tag{3}$$

D_1 is in proportion to the quantity of free charges Q_e on electrodes of piezoelectric ceramics, according to Maxwell's equations:

$$Q_e = \oiint_s D_1 ds = A_p \cdot D_1 \tag{4}$$

where A_p is the surface area of an electrode plate of piezoelectric stack. As the scale of deformation Δl is far smaller than the distance l between electrodes, Δl can be ignored and the electric field intensity E_1 can be regarded as linearly related to external driving voltage V:

$$E_1 = \frac{V}{l + \Delta l} \approx \frac{V}{l} \tag{5}$$

Substitute (4)(5) in (3), the relationship among strain S_1, free charge Q_e and voltage V can be written as:

$$S_1 = \frac{s_{11}}{d_{11}A_p} \cdot Q_e + (\frac{d_{11}}{l} - \frac{s_{11}\epsilon_{11}}{d_{11}l}) \cdot V \tag{6}$$

Because $\frac{s_{11}}{d_{11}A_p}$ and $(\frac{d_{11}}{l} - \frac{s_{11}\epsilon_{11}}{d_{11}l})$ are constants, the strain S_1 is a linear polynomial consisting Q_e and V. Design an approach to simultaneously measure the driving voltage and the quantity of free charges on one of the electrodes of PEA, then the increment of strain can be acquired as the displacement when the PEA stretches or retracts.

2) CIRCUIT DESIGN

A circuit shown in Fig.1 is designed for self-sensing measurement. A charge amplifier is used to measure the free charge on electrode of PEA. Theoretically, the PEA can be modeled as a capacitor C_p parallel connected with a charge source which applies Q_e on the polar plane of C_p. The charge induces equal quantity of charge on feedback capacitor C_f. According to $Q_e = C_p \cdot V_{driver} = C_f \cdot (-V_{out})$, the output voltage V_{out} can be used to denote the quantity of charge on an electrode of PEA.

However, piezoelectric ceramic in practice is not an ideal capacitor, but with a tiny current leaking through it when voltage is applied on. So the model is modified as the part inside dashed box in Fig.1. An equivalent resistor R_p with large resistance connects voltage source to the negative electrode of PEA and produces a current. Although the current leakage is small, it continuously charges the feedback capacitor C_f, causing drifting and aggravating the nonlinearity, which adds errors to measuring result. To relieve this problem, a leaking passage for current from R_p to get through without charging into C_f is established by parallel connecting a resistor R_l to C_f. The drift will be effectively slowed down if the resistance value of R_l is properly set. A high-precision operation amplifier with extremely low bias current is also selected for better linear performance. The quality of feedback capacitor also greatly influences the performance of charge amplifier, so precise capacitor with stable linearity under variable voltage should be selected as C_f.

A voltage follower circuit is used to transmit the actual driving voltage on PEA and prevent it being affected by sampling process. Besides being used as V in (6), the driving voltage also influences the rate of leakage through R_p. So it is also utilized to softly balance the drifting which can not be totally eliminated by hardware.

The output voltage V_{out} and the driving voltage V_{driver} are separately sampled by 18-bit A/D converters and then are transmitted to a MCU as original measurements, respectively denoting the Q_e and V in (6). Although the two voltages are theoretically unipolar, the A/D converters are set to bipolar mode to secure that voltages with tiny biases are also covered. That means only half of the sampling range is used, and effective A/D resolution is 17 bits. So the quantification error from A/D for a 0-3500nm measuring range is $\frac{1}{2} \times (3500nm/2^{17}) \approx 0.013nm$, which is far less than the error of the method itself and can be dismissed. Sampling and transmission period determines the frequency of self-sensing method, which is now locked as 10 times the sampling rate of TDC, about 250 Hz. Higher output rate can be achieved with more frequent data transmission.

3) COMPENSATION FOR LEAKAGE UTILIZING VOLTAGE

Beside hardware compensation for current leakage, a soft compensation utilizing the measuring result of actual driving voltage is adopted for better linearity. The current charging into C_p equals to:

$$I(t) = \frac{V_{driver}(t)}{R_p} - \frac{(-V_{out}(t))}{R_l} \tag{7}$$

So the actual output V_{out} contains two part of voltage, one caused by Q_e and the other caused by $I_(t)$:

$$-V_{out}(t) = (Q_e(t) + \int I(t)dt)/C_f \tag{8}$$

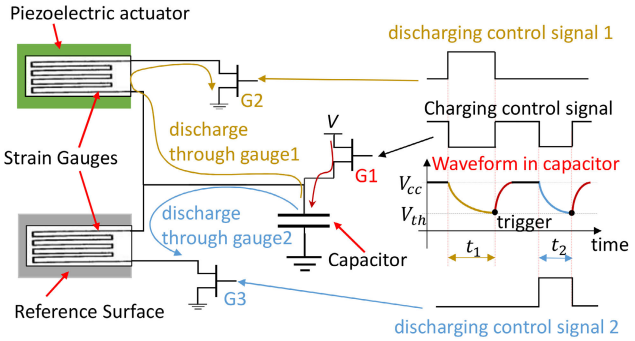

FIGURE 2. Principle of TDC. The difference of discharging time between two strain gauges indicates the displacement of PEA.

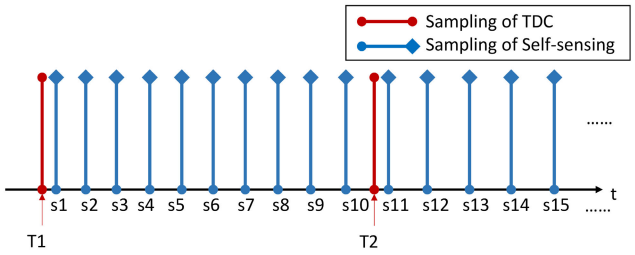

FIGURE 3. Sampling sequence of the two original measurements. Self-sensing is much faster than TDC.

So the real Q_e in discrete form can be written as:

$$Q_e(i) = C_f \cdot (-V_{out}(i)) - \sum_i \left(\frac{V_{driver}(i)}{R_p} - \frac{(-V_{out}(i))}{R_l}\right) \cdot \frac{1}{f} \quad (9)$$

where f is the sampling frequency of self-sensing. In this way the nonlinearity caused by current leakage can be further relieved.

B. TDC METHOD

As mentioned before, TDC is actually a strain gauge based method that measures displacement through measuring resistance of a deforming strain gauge. Different from other strain gauge based methods, TDC measures the resistance of strain gauge by measuring the time in which a capacitor is charged and discharged by current flowing through the strain gauge [11]. The strain gauge mounted on PEA changes its resistance when the PEA deforms, therefore changes the current flowing through it. Thus the time, in which this current charge or discharge a capacitor, can describe the displacement of PEA's deformation.

A half-bridge structure shown as Fig.2 is adopted to provide measurement with better accuracy and less affected by mechanical disturbance and temperature changing. Two strain gauges are used, one on objective PEA, the other on a fixed reference surface. The charging-discharging process are controlled by 3 switch transistors, the control signals of each are also shown in Fig.2. One period of measurement is composed of four steps: (1) the switch G1 is turned on while switches G2 and G3 are off, and the supply voltage $V(V \geq V_{cc})$ begins to charge the capacitor. When the voltage over the capacitor reaches V_{cc}, G1 is off and stops charging. (2) Then G2 switches on and the capacitor is discharged with current flowing through strain gauge on PEA until the voltage reaches bottom threshold V_{th}. The time step 2 takes is t_1. (3) Repeats step 1. (4) G3 switches on while G1 and G2 is off and the capacitor is discharged through strain gauge in reference surface. The time this step takes is t_2. Assume the resistances of strain gauges are R_p and R_{ref}, respectively for the one mounted on objective PEA and the one on reference surface, and the capacitance of the capacitor is C_{cap}, we have:

$$t_1 = R_p \cdot C_{cap} \cdot ln(\frac{V_{cc}}{V_{th}}) \quad (10)$$

$$t_2 = R_{ref} \cdot C_{cap} \cdot ln(\frac{V_{cc}}{V_{th}}) \quad (11)$$

The threshold voltages V_{cc} and V_{th} are fixed when the 4 steps are repeated for several periods to get an average result for one sample, and the same capacitor is used in two discharging stages, thus C_{cap}, V_{cc} and V_{th} can be considered as constants. Assume that the resistances of both strain gauges are influenced by a common environmental disturbance δ and that the resistance of the gauge on PEA changes ΔR_p because of the objective displacement, then there is:

$$\begin{aligned}\Delta t &= t_1 - t_2 \\ &= ((R_p + \Delta R_p + \delta) - (R_{ref} + \delta)) \cdot C_{cap} \cdot ln(\frac{V_{cc}}{V_{th}}) \\ &= \Delta R_p \cdot C_{cap} \cdot ln(\frac{V_{cc}}{V_{th}}) + (R_p - R_{ref}) \cdot C_{cap} \cdot ln(\frac{V_{cc}}{V_{th}}) \quad (12)\end{aligned}$$

All parameters on the right of equation (12) except ΔR_p are constants. As ΔR_p is proportional to displacement, the Δt is linear with displacement of PEA. Time-to-digit-converter with resolution as high as 15ps can precisely measure Δt to calculate displacement. As the time-counting device has no definite range, we directly use the true range of our measurements and its TDC readings' range to estimate quantification error from device, which is 0.044nm, also far less than the error of TDC itself and can be dismissed. Using the charging-discharging time measuring strategy, the current flowing through strain gauges can be very small, which is difficult to be precisely measured by other methods using A/D converters. As a result, the power dissipation of TDC is much lower than other strain gauge based methods. A calculation in [11] indicated that TDC dissipated nearly 90% less power than a traditional Wheatstone bridge taking the same parameters.

III. MULTI-RATE SENSOR FUSION

A fusion algorithm based on Kalman filter is used to fuse two measurements into one final measuring result, with the drawbacks of each minimized and their good characteristics maintained as possible. A main difficulty in our case is that the two measurements are asynchronous and TDC's sampling

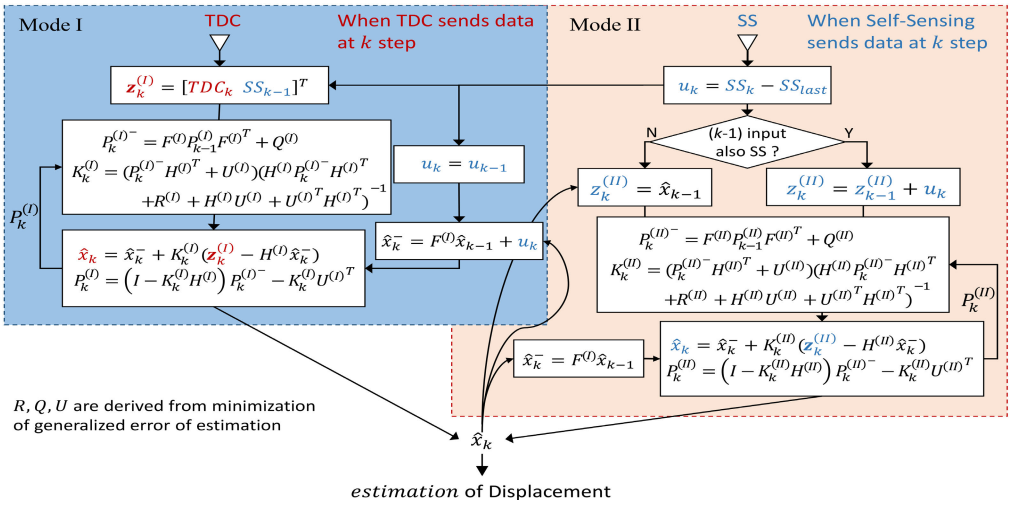

FIGURE 4. Diagram of fusion algorithm.

rate is significantly lower than self-sensing's, as Fig.3 shows, whereas we demand the frequency of fusion results not lower than the higher one. To solve this problem, a dual-modes mixed structure algorithm is used, as Fig.4 shows. Another problem is that measuring error is not only introduced by zero-mean Gaussian noises, which is the premise hypothesis of traditional Kalman filter, but also by deviation, which is caused by nonlinearity of measurements. This means, the mean square error(MSE) of sensors are not equal to the noise variance of measurements, so generalized errors are taken into consideration when determining parameters of Kalman filter.

A. STRUCTURE OF FUSION ALGORITHM

Fig.4 shows the structure of proposed fusion algorithm, which is built with two Kalman filters for different data sources, one working in mode I when measuring results of TDC come in, another working in mode II when self-sensing sends data. Combining data from measurements and from prediction model in each mode, displacement will be estimated according to a least-MSE oriented rule.

1) FUSION MODE I

When receiving measuring results from TDC in kth step, fusion algorithm processes the data in mode I, prediction is updated as:

$$\hat{x}_k^- = F^{(I)}\hat{x}_{k-1} + u_k \tag{13}$$

where model gain $F^{(I)} = 1$, $\hat{x}_k^-$ is a prediction based on the result of previous fusion step $\hat{x}_{k-1}$. As self-sensing's sampling rate is 10 times of TDC's, the $\hat{x}_{k-1}$ in mode I is usually a fusion output of mode II. The u_k is a predictive input, set equal to increment of self-sensing's measurement:

$$u_k = SS_{k-1} - SS_{k-2} \tag{14}$$

Here SS_i indicates the measuring result of self-sensing in step i ($i = k, k-1...$), and TDC_i will be used as indicator of TDC outputs in following equations. The superscript (I) indicates the parameters only work in mode I. The measurement $z_k^{(I)}$ is composed of fresh TDC measurement and the last input from self-sensing as

$$z_k^{(I)} = H^{(I)}x_k + v_k = [TDC_k \;\; SS_{k-1}]^T \tag{15}$$

where $H^{(I)} = [1\ 1]^T$ is the observation model gain, relating real state x_k to measurements $z_k^{(I)}$.

The updates of Kalman gain and error covariance are similar to classic Kalman filters, but slightly modified because v_k is no longer limited to zero-mean noises. The Kalman gain $K_k^{(I)}$ and error covariance $P_k^{(I)}$ are updated as below:

$$P_k^{(I)^-} = F^{(I)}P_{k-1}F^{(I)^T} + Q^{(I)} \tag{16}$$

$$K_k^{(I)} = (P_k^{(I)^-}H^{(I)^T} + U^{(I)})(H^{(I)}P_k^{(I)^-}H^{(I)^T} + R^{(I)} + H^{(I)}U^{(I)} + U^{(I)^T}H^{(I)^T})^{-1} \tag{17}$$

$$P_k^{(I)} = (1 - K_k^{(I)}H^{(I)})P_k^{(I)^-} - K_k^{(I)}U^{(I)^T} \tag{18}$$

$Q^{(I)}$ and $R^{(I)}$ respectively describe the accuracy of prediction model and of measurement, and $U_k^{(I)}$ is a new added parameter that does not exist in classic Kalman filter. All these parameters will be explained and educed in later section.

Finally the fusion result of current step $\hat{x}_k$ is calculated as a weighted mean of $\hat{x}_k^-$ and $z_k^{(I)}$:

$$\hat{x}_k = \hat{x}_k^- + K_k^{(I)}(z_k^{(I)} - H^{(I)}\hat{x}_k^-) \tag{19}$$

2) FUSION MODE II

When measuring results come from self-sensing, fusion process will be run in mode II. The prediction updates as:

$$\hat{x}_k^- = F^{(II)}\hat{x}_{k-1} \tag{20}$$

Here $F^{(II)} = 1$ but there is no need for a predictive input u_k this time. As same as in mode I, $\hat{x}_{k-1}$ is the fusion result

outputted by previous fusion step, which can come from mode I as well mode II. A major difference from mode I is that $z_k^{(II)}$ is not a direct measurement of either methods, but an accumulated result by increments of self-sensing measurement, starting from a base value. The base value will be renewed every time when mode changes from I to II, equal to previous estimation of mode I, with accumulation of increments cleared. That means, when mode I is switched to mode II, $z_k^{(II)}$ equals $\hat{x}_{k-1} + u_k$, otherwise if previous step is also in mode II, $z_k^{(II)}$ is added by u_k:

$$z_k^{(II)} = \begin{cases} \hat{x}_{k-1} + u_k, & \textit{previous step in mode I} \\ z_{k-1}^{(II)} + u_k, & \textit{previous step in mode II} \end{cases} \tag{21}$$

The updates of Kalman gain $K_k^{(II)}$ and error covariance $P_k^{(II)}$ in mode II are same as mode I, that is

$$P_k^{(II)^-} = F^{(II)} P_{k-1} F^{(II)^T} + Q^{(II)} \tag{22}$$

$$K_k^{(II)} = (P_k^{(II)^-} H^{(II)^T} + U^{(II)})(H^{(II)} P_k^{(II)^-} H^{(II)^T} + R^{(II)} + H^{(II)} U^{(II)} + U^{(II)^T} H^{(II)^T})^{-1} \tag{23}$$

$$P_k^{(II)} = (1 - K_k^{(II)} H^{(II)}) P_k^{(II)^-} - K_k^{(II)} U^{(II)^T} \tag{24}$$

Finally the fusion result of current step $\hat{x}_k$ is calculated as:

$$\hat{x}_k = \hat{x}_k^- + K_k^{(II)}(z_k^{(II)} - H^{(II)} \hat{x}_k^-) \tag{25}$$

B. DETERMINATION OF FUSION PARAMETERS

The main settable parameters in classic Kalman filter are measurement noise covariance R and process noise covariance Q respectively of sensors and prediction model. R can be acquired by sensor testing, but Q for prediction model is hard to exactly know, therefore it is usually a parameter adjusted until getting best fusion performance. In classic Kalman filtering, the error of a sensor is assumed to be introduced totally by zero-mean Gaussian noises, so the variance of noise is used as R. But in nano-scale, deviation of measuring is unavoidable, which usually causes bigger errors than noise does, so only considering noises when calculating R is not enough. It is necessary to start from the origin of Kalman filtering with the participation of generalized errors.

1) DERIVATION

The original purpose of Kalman filtering is to minimize the mean square error(MSE) of fusion result:

$$P_k = E[(x_k - \hat{x}_k)(x_k - \hat{x}_k)^T] \tag{26}$$

The sum of diagonal elements of P_k, also the trace of the matrix, is the MSE of fusion result to be minimized. According to fusion formula $\hat{x}_k = \hat{x}_k^- + K_k(z_k - H\hat{x}_k^-)$ and measurement model $z_k = Hx_k + v_k$, P_k can be expanded as

$$\begin{aligned} P_k &= E[((I - K_k H)(x_k - \hat{x}_k^-) - K_k v_k)((I - K_k H)(x_k - \hat{x}_k^-) - K_k v_k)^T] \\ &= K_k H P_k^- H^T K_k^T - K_k H P_k^- - P_k^- H^T K_k^T + P_k^- \\ &\quad - K_k U^T + K_k U^T H^T K_k^T - U K_k^T + K_k H_k U K_k^T \\ &\quad + K_k R K_k^T \end{aligned} \tag{27}$$

Here P_k^- is covariance matrix of prediction, R actually reflects MSE of sensor, U is the mathematical expectation for product of the errors from prediction model and from sensor, but not the covariance:

$$P_k^- = E[(x_k - \hat{x}_k^-)(x_k - \hat{x}_k^-)^T] \tag{28}$$

$$R = E[v_k v_k^T] \tag{29}$$

$$U = E[(x_k - \hat{x}_k^-) v_k^T] \tag{30}$$

v_k is the generalized error between measurements and true values, including errors caused by noises, deviations or other factors. Because model error and sensor error are independent, so (30) can be further expand as $U = E[x_k - \hat{x}_k^-] \cdot E[v_k^T]$. Therefore if v_k is a zero-mean noise, then $U = 0$, R equals to noise's covariance and the expression of P_k will be turned into form of classic Kalman filter. To minimize the MSE of fusion result, take the derivative of the trace of P_k:

$$\frac{d\ Tr(P_k)}{d\ K_k} = 2K_k(HP_k^- H^T + R + HU + U^T H^T) - 2P_K^{-T} H^T - 2U \tag{31}$$

Set (31) to 0 then

$$K_k = (P_k^- H^T + U)(HP_k^- H^T + R + HU + U^T H^T)^{-1} \tag{32}$$

Substitute K_k with (32) in (27), we have:

$$P_k = (I - K_k H) P_k^- - K_k U^T \tag{33}$$

The prediction model error can be described with help of recurrence model:

$$\begin{aligned} x_k - \hat{x}_k^- &= F_k x_{k-1} + B u_k + w_k - (F_k \hat{x}_{k-1} + B u_k) \\ &= F_k(x_{k-1} - \hat{x}_{k-1}) + w_k \end{aligned} \tag{34}$$

Then the expression for P_k^- is rewrote as:

$$\begin{aligned} P_k^- &= E[(x_k - \hat{x}_k^-)(x_k - \hat{x}_k^-)^T] \\ &= F_k E[(x_{k-1} - \hat{x}_{k-1})(x_{k-1} - \hat{x}_{k-1})^T] F_k^T \\ &\quad + F_k E[(x_{k-1} - \hat{x}_{k-1}) w_k^T] + E[w_k (x_{k-1} \\ &\quad - \hat{x}_{k-1})^T] F_k^T + E(w_k w_k^T) \end{aligned} \tag{35}$$

w_k is the model error, then $E(w_k w_k^T)$ is the Q in Kalman filtering. And $(x_{k-1} - \hat{x}_{k-1})$ happens to be the fusion error of the previous step, then the MSE in first term of (35) is P_{k-1}. $(x_{k-1} - \hat{x}_{k-1})$ is independent from w_k and its mathematical expectation is zero because the fusion result should not deviates from true value. Then (35) can be further simplified and we get the recursive formula for P_k^- as same as classic Kalman filter:

$$\begin{aligned} P_k^- &= F_k P_{k-1} F_k^T + 0 \cdot E[w_k^T] + E[w_k] \cdot 0 + Q \\ &= F_k P_{k-1} F_k^T + Q \end{aligned} \tag{36}$$

Now (36)(32)(27) constitute the parameter updates of mode I. Among settable parameters, R and U both can be calculated with sensor testing data. Actually the U in real cases is very small and may be ignored, which turns the updating formulas into traditional form, but with different meaning of R. So the main difference this derivation made,

is replacing the sensor noises with sensor errors when calculating R, which are regarded as equal in most cases but can result in big difference in nano-scale measurement.

In mode I, $R^{(I)}$ is a matrix consisting of MSE of self-sensing and TDC, while in mode II geometric mean of self-sensing's and formerly tested fusion result's MSE is used as $R^{(II)}$, because the 'measurement' in mode II is based on both self-sensing measurement and previous fusion result.

2) SELF-ADAPTIVE PARAMETER Q

Q can be set as a constant that makes the fusion error as small as possible. Fixed value for $Q^{(I)}$ may cause fusion result distorted in some certain condition, where the the algorithm depends on prediction to a considerable extent, which may cause fusion result hard to keep pace with the changes of object, if it is very rapid. So $Q^{(I)}$ is modified with a punishment function, adaptively securing the algorithm from fatal deviation:

$$Q^{(I)} = Q_0 + C \cdot e^2(1 + \frac{e-1}{|e|+1}) \tag{37}$$

Here Q_0 and C are constants, $e = (TDC_k - \hat{x}_k^-)\cdot(SS_{k-1} - \hat{x}_k^-)$. If fusion result deviates from the two measurements in same side, $Q^{(I)}$ will increase rapidly when the errors get larger, then the algorithm will depend more on measurements rather than prediction and vice versa. The distortion will be prevented in this way, improving stability in dynamic situations.

IV. EXPERIMENTS

A. EXPERIMENTS SETUP

1) SYSTEM SETUP

The experimental system are configured as Fig.5: a stack PEA is fixed on a metal base with an end free for movement. It is driven by a voltage varying in range of $0 \sim 60$V with peak-to-peak ripples less than 10 mV. The voltage can be manually adjusted or controlled by waveform signal from PC.

The self-sensing circuit is directly embedded in supply loop of the PEA and the TDC processing circuit is connected to a half-bridge consisting of 2 strain gauges that are separately mounted on the surface of PEA and on a reference surface as mentioned in previous section. The original data is transmitted through SPI bus to MCU where the data is processed into measurements and then is sent to PC for further fusion and evaluation.

A laser interferometer (SIOS SP2000 TR) with a resolution of 0.1nm is used to provide standard measurement as contrast. As auxiliary, a mirror is secured to the free end of PEA, perpendicular to the direction of measured displacement, reflecting the laser back into the laser receiver.

All the components of the system except the PC are placed on a vibration isolation table inside a chamber to minimize external disturbance.

2) SENSOR CALIBRATION

The TDC outputs a digit y denoting the Δt in (12), and the Self-sensing provides measurements in form of two voltage

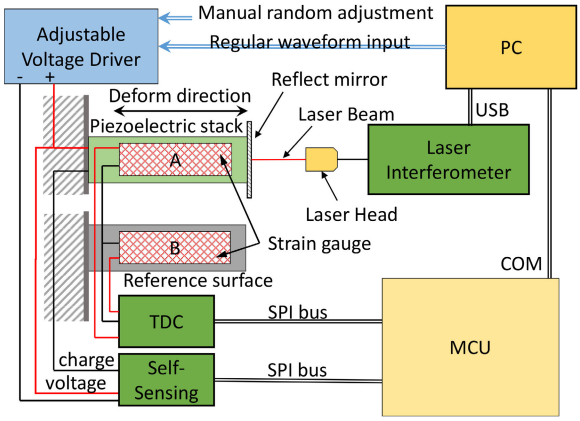

FIGURE 5. Experiment setup.

readings $x = [v_1, v_2]'$, denoting Q_e and V_{driver}, separately. According to (6) and (12), the original measurements should be calibrated into the scale of true displacement in following linear relationships:

$$z_1 = A_1 \cdot x + b_1 \tag{38}$$
$$z_2 = a_2 \cdot y + b_2 \tag{39}$$

With TDC, self-sensing and interferometer, simultaneous measurements are conducted in which the PEA is driven by a varying voltage covering full range of output. With sufficient raw data of the three measurements, the parameter in (38)(39) can be estimated by least square method. Assume in sampling test self-sensing outputted n data pairs $x_s = [v_{11}, v_{12}, \ldots, v_{1n}; v_{21}, v_{22}, \ldots, v_{2n}]$ and TDC outputs m readings $y_t = [y_1, y_2, \ldots, y_m]$, with corresponding interferometer readings $z_1 = [z_{11}, \ldots, z_{1n}]$ and $z_2 = [z_{21}, \ldots, z_{2m}]$, we have:

$$A_1 = (\frac{1}{n} z_1 x_s^T - \overline{z_1}\,\overline{x_s^T})(\frac{1}{n} x_s x_s^T - \overline{x_s}\,\overline{x_s^T})^{-1} \tag{40}$$
$$b_1 = \overline{z_1} - A_1 \overline{x_s} \tag{41}$$
$$a_2 = \frac{\overline{y_t \cdot z_2^T} - \overline{y_t}\cdot\overline{z_2}}{\overline{y_t y_t^T} - \overline{y_t}^2} \tag{42}$$
$$b_2 = \overline{z_2} - a_2 \overline{y_t} \tag{43}$$

where $\overline{x_s} = [\overline{v_1}, \overline{v_2}]^T$. With measurements calibrated, following experiments can be conducted with online fusion, to evaluate the proposed methods.

B. PERFORMANCE EVALUATION

1) LINEARITY

Linearity indicates the extent to which the measured curve deviate from ideal curve over measuring range [33]. To evaluate the methods in a relative general situation, the PEA is driven by a $0 \sim 60$V voltage in a casually adjusted irregular waveform.

The measurements against time are compared in Fig.6. As Fig.6 shows, the curves of proposed methods are highly

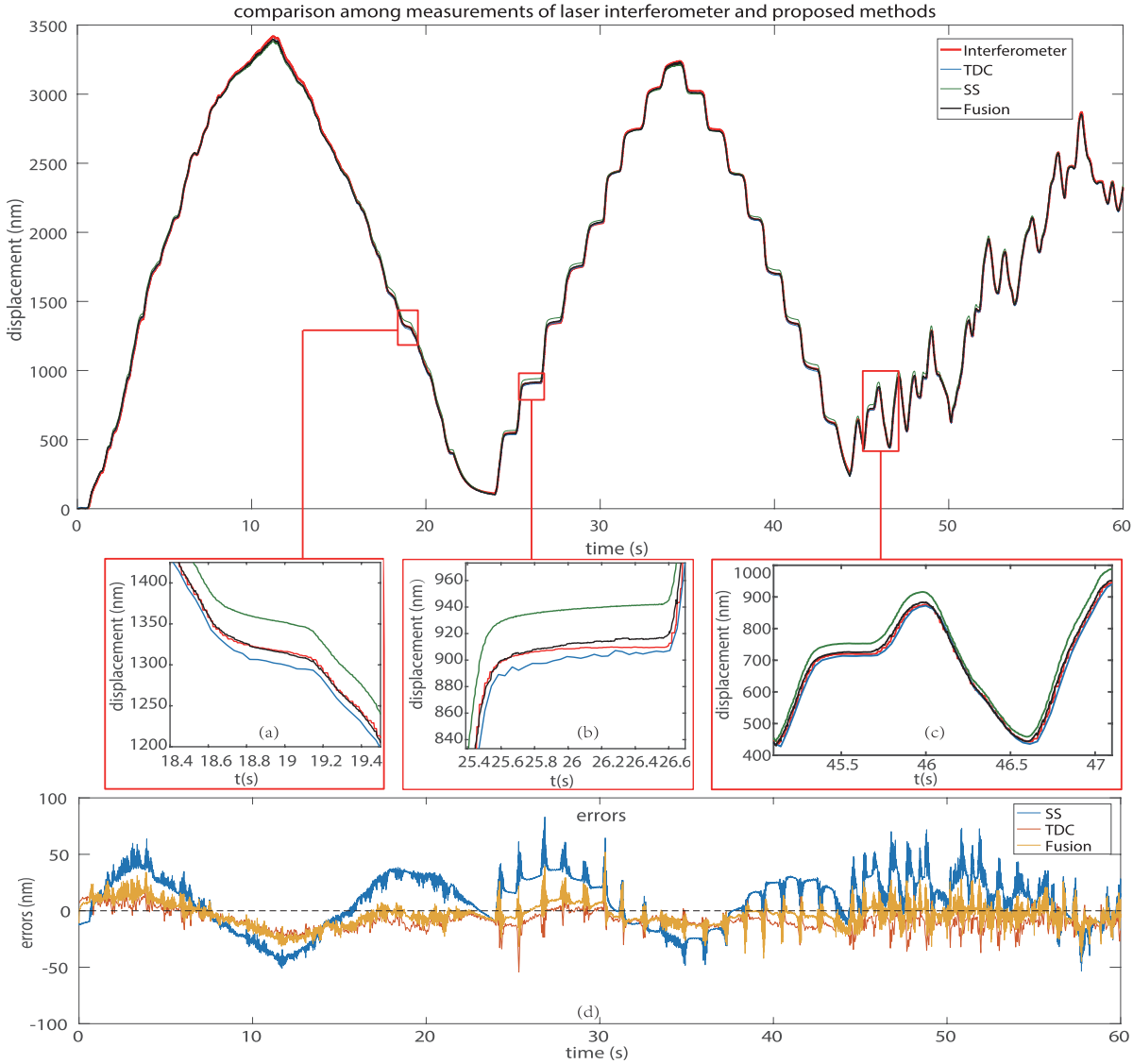

FIGURE 6. **Comparison among measurements of interferometer and proposed methods on randomly adjusted displacement, in 60s' full-range experiment. (a)(b) and (c) shows some typical situation where one of the original measurements greatly deviates from true value, the fusion result still stays close to it. (d) presents errors of the methods along time.**

close to the curve of true value which is provided by laser interferometer. Subplots (a)(b) and (c) present zoomed views of some typical parts where one of original measurements deviates far from true values. Because of heavier nonlinearity, self-sensing method deviates more than TDC does, which is clearly shown by the error curves in (d). However, the fusion successfully relieves the influence of nonlinearity, making the result close to true value as possible. It also can be noticed that when a sharp change of displacement happens, there are corresponding pulses occurring in error curves. And the directions of pulses are basically converse for TDC and self-sensing. The phenomenon is mostly ascribed to the time lags among the samplings of TDC, self-sensing and interferometer. As the sampling rate of TDC is very low, its measurement is usually delayed when displacement changes too rapidly, so there will be error pulses occurring in converse direction of displacement's upheavals. On the contrary, error pulses of self-sensing indicate that its measurement is ahead of interferometer's. One reason is that interferometer updates its measurement more slowly than self-sensing, but system requests measurement in same rate of self-sensing, so it has to output outdated data in buffers, making the errors bigger than it actually be. Another potential reason is that self-sensing may predictively sense the displacement which does not yet mechanically occurs. The fusion effectively reduces errors of original measurements in general, though in some cases the fusion result is slightly worse than one of the measurements. This mostly happens where TDC and Self-sensing deviate toward same direction, as the fusion in substance is a balance between two data sources after all. Anyway, the fusion result

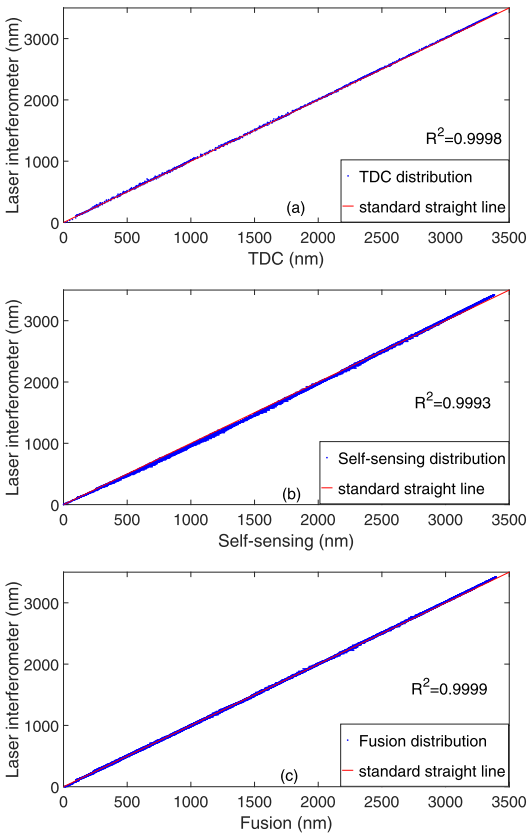

FIGURE 7. The distribution of measurements of proposed methods, plotted against the measurements of laser interferometer.

TABLE 1. Performances comparison.

	Self-sensing	TDC	Fusion Result
R^2	0.9993	0.9998	0.9999
Avg. Error(abs)	21.3nm	10.2nm	9.0nm
RMSE	24.9nm	12.1nm	10.9nm
sampling rate	244Hz	24Hz	268Hz

achieves an average absolute error of 9.0nm and a root mean square error(RMSE) of 10.9nm, better than both self-sensing and TDC.

Fig.7 plots the measurements of proposed methods against true value provided by interferometer. The more the plotted points close to standard straight line, the better the linearity is. Linear coefficient of determination R^2 is also adopted as an indicator of linearity. In Fig.7, the two original measurements as well as the fusion result have deviation to some extent, and the self-sensing has worst linearity with $R^2 = 0.9993$ while TDC's $R^2 = 0.9998$. The fusion improves the linearity of self-sensing greatly and even gets better linearity than TDC as its $R^2 = 0.9999$. The comparison of linear performance are presented in TABLE 1.

Displacement changing in regular waveform with higher changing frequency is also measured for tests. Fig.8 displays the situation where modulated sinusoidal wave is applied on PEA.

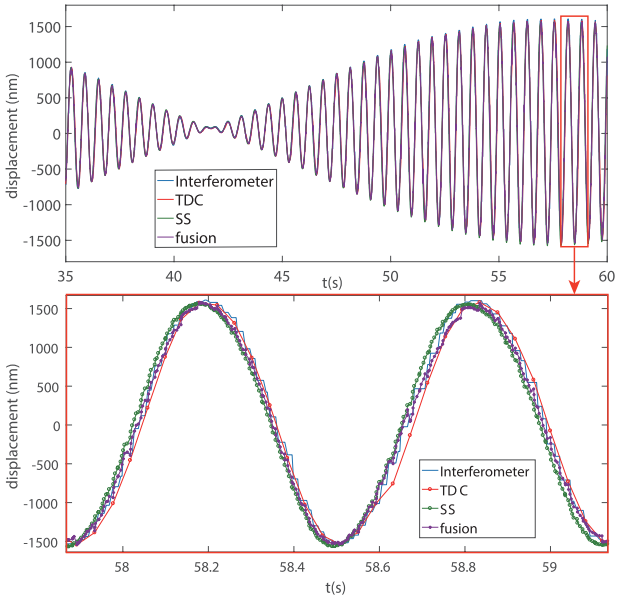

FIGURE 8. Measurements for displacement in modulated sinusoidal waveform.

TABLE 2. Results comparison when objective actuator deformed in high frequency.

	Self-sensing	TDC	Fusion Result
R^2	0.9784	0.9891	0.9896
Avg. Error(abs)	76.9nm	48.8nm	50.0nm
RMSE	107.7nm	76.8nm	73.1nm

As displacement changes in higher frequency, the errors of all the measurements are greatly aggravated, mainly by time lags between samplings of each method and interferometer, although the curves of these measurements still keep close to the curve of true value. The results are listed in TABLE 2, where the fusion result still achieves relatively better performance in general.

2) RESOLUTION

Resolution is the minimum distance between adjacent but unique locations, so it must be larger than noise to avoid mistaking one point for the other [34]. The noise, which is the determinant of resolution, can be estimated through time-domain information. The voltage is increased to and fixed at about half of the maximal voltage, nearly 30V. Then noises of proposed methods can be acquired by subtracting sliding-filtered signals from raw data, as Fig.9 shows. It is obvious that self-sensing has smallest noise, thus its resolution is best among the three. Noise can be introduced by electrical disturbances through some components and circuit structure, but self-sensing data is sampled in an electrode of feedback capacitor which filters some noises already; while TDC also suffers from mechanical disturbances in contact surface between strain gauge and PEA, so the resolution of self-sensing is far better than TDC. The result after fusion, though suffers some aggravation compared to self-sensing, still obviously excels TDC in resolution.

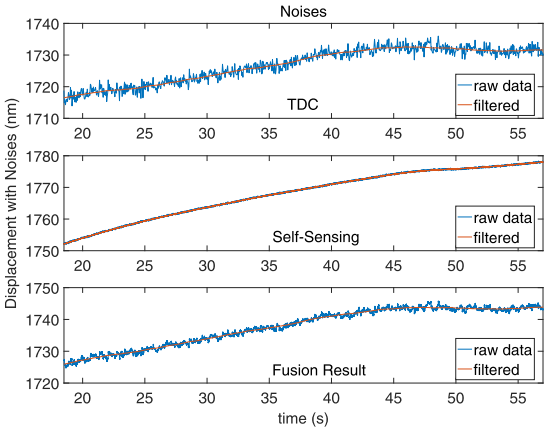

FIGURE 9. **Comparison of noises.**

To quantify the performance, 6σ-form is adopted to describe resolution, where σ is the root mean square (RMS) value of noise. As the sampling rates are fixed, all the RMS value are acquired in sensors' effective bandwidth which is half of the sampling rate of each. The 6σ resolution is about 6.1nm at 12Hz for TDC, 0.6nm at 122Hz for self-sensing and 3.2nm at 134Hz for fusion result.

V. CONCLUSION

In this paper, a measurement for piezoelectric displacement is proposed, combining the TDC and self-sensing methods. A dual-mode Kalman filter considering generalized errors is designed for the two sensing methods with different sampling rates to be fused. Several experiments are conducted to test the effectiveness of the fused measurement, which achieves a sampling rates of 268Hz with resolution of 3.2nm. And a linearity up to 0.9999 is achieved throughout 3500nm range. As the dual-mode fusion gives estimation whenever and wherever a raw measurement is acquired, it will still work effectively when changes happen to inputing frequency. So the sampling rate of final measurement can be further increased just by improving self-sensing's transmission. The results demonstrate that the method is capable of providing displacement feedbacks for positioning applications.

REFERENCES

[1] C. Shi, D. K. Luu, Q. Yang, J. Liu, J. Chen, C. Ru, S. Xie, J. Luo, J. Ge, and Y. Sun, "Recent advances in nanorobotic manipulation inside scanning electron microscopes," *Microsyst. Nanoeng.*, vol. 2, Jun. 2016, Art. no. 16024.

[2] C. Zhou, Z. Gong, B. K. Chen, Z. Cao, J. Yu, C. Ru, M. Tan, S. Xie, and Y. Sun, "A closed-loop controlled nanomanipulation system for probing nanostructures inside scanning electron microscopes," *IEEE/ASME Trans. Mechatronics*, vol. 21, no. 3, pp. 1233–1241, Jun. 2016.

[3] C. Ru, Y. Zhang, Y. Sun, Y. Zhong, X. Sun, D. Hoyle, and I. Cotton, "Automated four-point probe measurement of nanowires inside a scanning electron microscope," *IEEE Trans. Nanotechnol.*, vol. 10, no. 4, pp. 674–681, Jul. 2011.

[4] S. C. Lim, K. S. Kim, S. Y. Jeong, S. Cho, J.-E. Yoo, and Y. H. Lee, "Nanomanipulator-assisted fabrication and characterization of carbon nanotubes inside scanning electron microscope," *Micron*, vol. 36, no. 5, pp. 471–476, Jul. 2005.

[5] M. Yu, M. J. Dyer, G. D. Skidmore, H. W. Rohrs, X. Lu, K. D. Ausman, J. R. Von Ehr, and R. S. Ruoff, "Three-dimensional manipulation of carbon nanotubes under a scanning electron microscope," *Nanotechnology*, vol. 10, no. 3, p. 244, Sep. 1999.

[6] T. Fukuda, F. Arai, and L. Dong, "Assembly of nanodevices with carbon nanotubes through nanorobotic manipulations," *Proc. IEEE*, vol. 91, no. 11, pp. 1803–1818, Nov. 2003.

[7] Y. Liu, J. Deng, and Q. Su, "Review on multi-degree-of-freedom piezoelectric motion stage," *IEEE Access*, vol. 6, pp. 59986–60004, 2018.

[8] H. Yan, H.-Z. Duan, L.-T. Li, Y.-R. Liang, J. Luo, and H.-C. Yeh, "A dual-heterodyne laser interferometer for simultaneous measurement of linear and angular displacements," *Rev. Sci. Instrum.*, vol. 86, no. 12, Dec. 2015, Art. no. 123102.

[9] H. Qu, G. F. Yan, and M. Skorobogatiy, "Interferometric fiber-optic bending/nano-displacement sensor using plastic dual-core fiber," *Opt. Lett.*, vol. 39, no. 16, pp. 4835–4838, Aug. 2014.

[10] J. N. Dash, R. Jha, J. Villatoro, and S. Dass, "Nano-displacement sensor based on photonic crystal fiber modal interferometer," *Opt. Lett.*, vol. 40, no. 4, pp. 467–470, Feb. 2015.

[11] C. Zhou, Y. Wang, L. Deng, Z. Wu, Z. Cao, S. Wang, and M. Tan, "A TDC-based nano-scale displacement measure method inside scanning electron microscopes," in *Proc. IEEE Int. Conf. Robot. Biomimetics*, Qingdao, China, Dec. 2016, pp. 1298–1302.

[12] B. George, Z. Tan, and S. Nihtianov, "Advances in capacitive, eddy current, and magnetic displacement sensors and corresponding interfaces," *IEEE Trans. Ind. Electron.*, vol. 64, no. 12, pp. 9595–9607, Dec. 2017.

[13] S. Rombach, M. Marx, S. Gu-Stoppel, and Y. Manoli, "Low power closed-loop driving circuit for piezoelectric microscanners based on tuneable capacitive position sensors," *Procedia Eng.*, vol. 120, pp. 63–66, Sep. 2015.

[14] Y. L. Zhang, Y. Zhang, C. Ru, B. K. Chen, and Y. Sun, "A load-lock-compatible nanomanipulation system for scanning electron microscope," *IEEE/ASME Trans. Mechatronics*, vol. 18, no. 1, pp. 230–237, Feb. 2013.

[15] B. Jaffe, *Piezoelectric Ceramics*, 1st ed. London, U.K.: Academic, 1971.

[16] A. Furuta, M. Munekata, and T. Higuchi, "Precise positioning stage driven by multilayer piezo actuator using strain gauge," *Jpn. J. Appl. Phys.*, vol. 41, p. 6283, Oct. 2002.

[17] H. Huang, H. Zhao, Z. Yang, Z. Fan, S. Wan, C. Shi, and Z. Ma, "Design and analysis of a compact precision positioning platform integrating strain gauges and the piezoactuator," *Sensors*, vol. 12, pp. 9697–9710, Jul. 2012.

[18] L. Jones, E. Garcia, and H. Waites, "Self-sensing control as applied to a pzt stack actuator used as a micropositioner," *Smart Mater. Struct.*, vol. 3, no. 2, p. 147, Feb. 1994.

[19] I. A. Ivan, M. Rakotondrabe, P. Lutz, and N. Chaillet, "Quasistatic displacement self-sensing method for cantilevered piezoelectric actuators," *Rev. Sci. Instrum.*, vol. 80, no. 6, Jun. 2009, Art. no. 065102.

[20] M. N. Islam and R. J. Seethaler, "Sensorless position control for piezoelectric actuators using a hybrid position observer," *IEEE/ASME Trans. Mechatronics*, vol. 19, no. 2, pp. 667–675, Apr. 2014.

[21] B. Ju, Z. Guo, Y. Liu, G. Qian, L. Xu, and G. Li, "Self-sensing vibration suppression of piezoelectric cantilever beam based on imporved mirror circuit," *IEEE Access*, vol. 7, pp. 148381–148392, 2019.

[22] M. Ling, J. Cao, Q. Li, and J. Zhuang, "Design, pseudostatic model, and PVDF-based motion sensing of a Piezo-actuated XYZ flexure manipulator," *IEEE/ASME Trans. Mechatronics*, vol. 23, no. 6, pp. 2837–2848, Dec. 2018.

[23] M. Rakotondrabe, "Combining self-sensing with an unkown-input-observer to estimate the displacement, the force and the state in piezoelectric cantilevered actuators," in *Proc. IEEE Amer. Control Conf.*, Washington, DC, USA, Jun. 2013, pp. 4523–4530.

[24] K.-H. Oh and H.-S. Ahn, "Extended Kalman filter with multi-frequency reference data for quadrotor navigation," in *Proc. IEEE 15th Int. Conf. Control Automat. Syst.*, Busan, South Korea, Oct. 2015, pp. 201–206.

[25] A. Smyth and M. Wu, "Multi-rate Kalman filtering for the data fusion of displacement and acceleration response measurements in dynamic system monitoring," *Mech. Syst. Signal Process.*, vol. 21, no. 2, pp. 706–723, Feb. 2007.

[26] K. Kim, J. Choi, G. Koo, and H. Sohn, "Dynamic displacement estimation by fusing biased high-sampling rate acceleration and low-sampling rate displacement measurements using two-stage Kalman estimator," *Smart Struct. Syst.*, vol. 17, no. 4, pp. 647–667, Apr. 2016.

[27] Y. Wang, Y. Liu, H. Fujimoto, and Y. Hori, "Vision-based lateral state estimation for integrated control of automated vehicles considering multirate and unevenly delayed measurements," *IEEE/ASME Trans. Mechatronics*, vol. 23, no. 6, pp. 2619–2627, Dec. 2018.
[28] L. Yan, B. Liu, and D. Zhou, "Asynchronous multirate multisensor information fusion algorithm," *IEEE Trans. Aerosp. Electron. Syst.*, vol. 43, no. 3, Jul. 2007.
[29] S. Safari, F. Shabani, and D. Simon, "Multirate multisensor data fusion for linear systems using Kalman filters and a neural network," *Aerosp. Sci. Technol.*, vol. 39, pp. 465–471, Dec. 2014.
[30] *Standard on Piezoelectricity*, IEEE Standard 176, 1987.
[31] J. A. Main, E. Garcia, and D. V. Newton, "Precision position control of piezoelectric actuators using charge feedback," *J. Guid., Control, Dyn.*, vol. 18, no. 5, pp. 1068–1073, Sep. 1995.
[32] Z. Du, T. Zhang, L. Deng, C. Zhou, Z. Cao, and S. Wang, "A charge-amplifier based self-sensing method for measurement of piezoelectric displacement," in *Proc. IEEE Int. Conf. Mechatronics Automat.*, Takamatsu, Japan, Aug. 2017, pp. 1995–1999.
[33] J. J. Carr and J. M. Brown, *Introduction to Biomedical Equipment Technology*, 3rd ed. Upper Saddle River, NJ, USA: Prentice-Hall, 1998.
[34] A. J. Fleming, "A review of nanometer resolution position sensors: Operation and performance," *Sens. Actuators A, Phys.*, vol. 190, pp. 106–126, Feb. 2013.

ZHANGMING DU received the B.E. degree in control theory and control engineering from Zhejiang University, Hangzhou, China, in July 2015. He is currently pursuing the joint Ph.D. degree in control theory and control engineering with the Institute of Automation, Chinese Academy of Sciences, and also with the University of Chinese Academy of Sciences, Beijing.

His research interests include measurements, intelligent control, and nano/microrobots.

CHAO ZHOU received the B.S. degree (Hons.) in automation from Southeast University, Nanjing, China, in July 2003, and the Ph.D. degree in control theory and control engineering from the Institute of Automation, Chinese Academy of Sciences, Beijing, China, in 2008.

He is currently a Professor with the State Key Laboratory of Management and Control for Complex Systems, Institute of Automation, Chinese Academy of Sciences. His current research interests include the motion control of robot, the bio-inspired robotic fish, and embedded systems of robot.

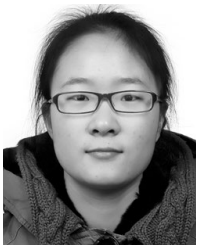

TIANLU ZHANG received the B.E. degree from the Beijing University of Chemical Technology, Beijing, China, in July 2017. She is currently pursuing the joint M.E. degree in control theory and control engineering with the Institute of Automation, Chinese Academy of Sciences, and also with the University of Chinese Academy of Sciences, Beijing.

Her research interests include nano/microrobots, piezoelectric actuator, and intelligent control.

LU DENG received the B.S. degree of international economics and trade and the M.S. degree of econometrics from the Hebei University of Technology, Tianjin, China, in July 2003 and March 2006, respectively, and the Ph.D. degree in econometrics from the Nankai University, Tianjin, in 2009. Since July 2009, she has been an Assistant Professor with the Central University of Finance and Economics, where she has also been an Associate Professor, since October 2011. Her current research interests include error analysis, time series modeling, and complex data.

ZHIQIANG CAO (SM'14) received the B.S. degree in automation and the M.S. degree in control theory and control engineering from the Shandong University of Technology, Jinan, China, in 1996 and 1999, respectively, and the Ph.D. degree in control theory and control engineering from the Institute of Automation, Chinese Academy of Sciences, Beijing, China, in 2002.

He is currently a Professor with the State Key Laboratory of Management and Control for Complex Systems, Institute of Automation, Chinese Academy of Sciences. His research interests include environmental cognition, service robot, and multirobot coordination.

LONG CHENG (SM'14) received the B.S. degree (Hons.) in control engineering from Nankai University, Tianjin, China, in July 2004, and the Ph.D. degree (Hons.) in control theory and control engineering from the Institute of Automation, Chinese Academy of Sciences, Beijing, China, in July 2009.

He is currently a Full Professor with the Laboratory of Complex Systems and Intelligent Science, Institute of Automation, Chinese Academy of Sciences. He is also an Adjunct Professor with the University of the Chinese Academy of Sciences. His current research interests include intelligent control of smart materials, coordination of multiagent systems, and neural networks and their applications to robotics.